Integrated Brain Atlas for Unbiased Mapping of Nervous System Effects Following Liraglutide Treatment

Casper Bo Jensen[1,2], Tess Tsai-Hsiu Lu[1], Sanaz Gabery[1], Kasper Marstal[2,4], Tomas Alanentalo[1], Aaron Jeffrey Mercer[3], Anda Cornea[3], Knut Conradsen[2], Jacob Hecksher-Soerensen[1], Anders Bjorholm Dahl[2], Lotte Bjerre Knudsen*[1], Anna Secher[1]

[1]Global Research, Novo Nordisk A/S, Måløv, Denmark;

[2]Image Analysis & Computer Graphics, Department of Applied Mathematics and Computer Science , Technical University of Denmark, Kgs. Lyngby, Denmark;

[3]Global Research, Novo Nordisk A/S, Seattle, USA;

[4]Biomedical Imaging Group Rotterdam (BIGR), Department of Radiology & Medical Informatics, Erasmus Medical Center, Rotterdam, Netherlands;

*Contact:

Lotte Bjerre Knudsen - lbkn@novonordisk.com

Novo Nordisk A/S, Novo Nordisk Park, DK-2760 Maaloev, Denmark.

Supplementary Figures

Integrated Brain Atlas for Unbiased Mapping of Nervous System Effects Following Liraglutide Treatment

- S1. **Image registration**
- S2. **Accuracy of image registration**
- S3. **Unmix signals**
- S4. **Average brain signals**
- S5. **Confocal images of liraglutide^{Cy3}**
- S6. **Enhanced ISH images**
- S7. **Liraglutide^{VT750} in wild type vs *Glp-1r*$^{-/-}$ mice**
- S8. **c-Fos heat maps**
- S9. **Rank plot**

S1. **Image registration**

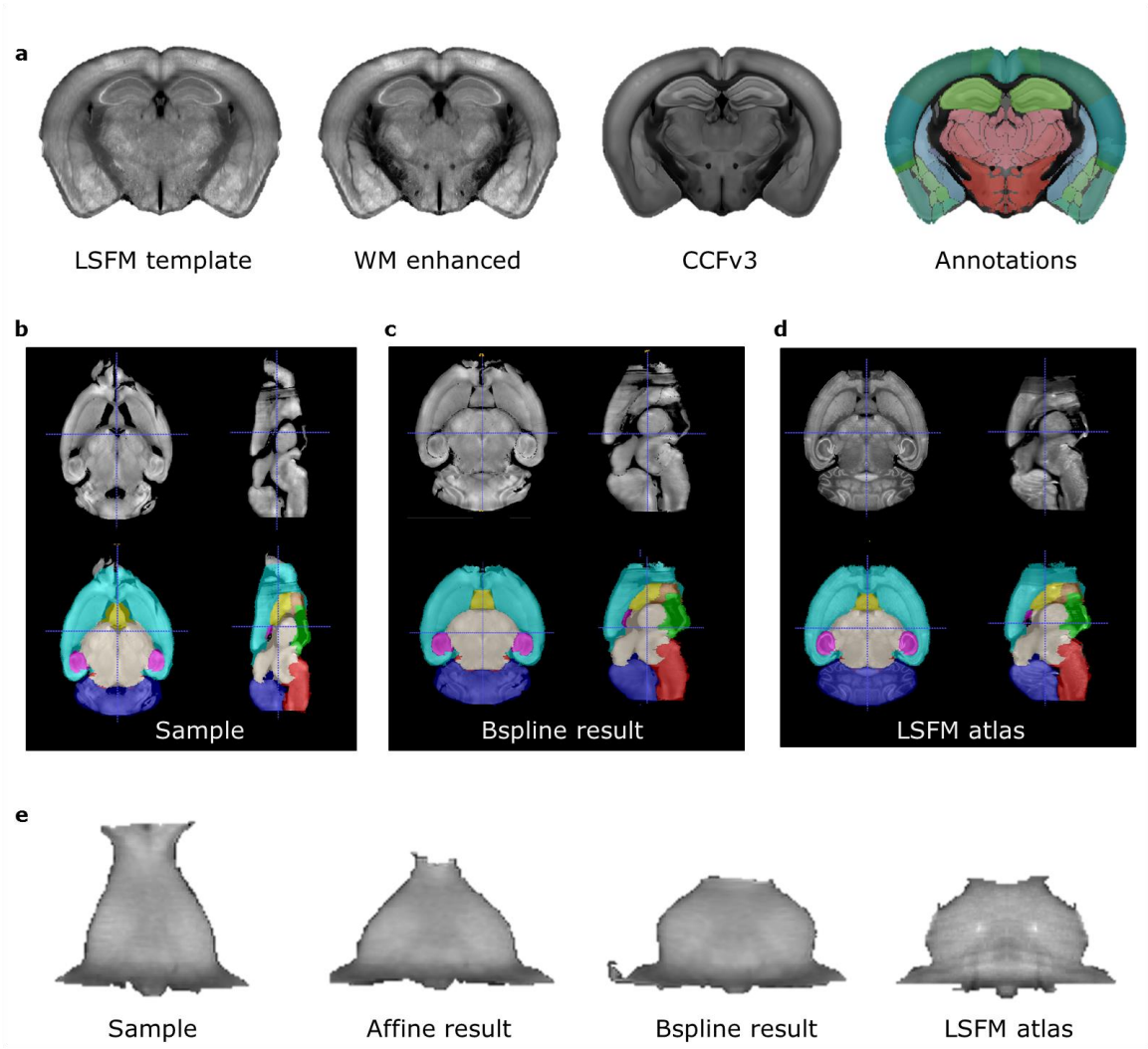

Supplement Figure 1 I Image registration. (**a**) A LSFM template was constructed from a representative C57Bl/6J male mouse by registration of the brain to the CCFv3 atlas[7] from AIBS. A white matter (WM) enhanced version of the LSFM template was constructed to increase the alignment quality. (**b**) Example of a brain sample to be registered to the LSFM template of the integrated brain atlas. Large deformations have occurred during the tissue processing prior to imaging. (**c**) The result of aligning the sample to the LSFM atlas. The registration was performed in separate parts to mitigate the large deformations. Separate affine and b-spline registration was performed for ten larger structures, here visualized by the overlay colours in the lower part of the figure. (**d**) LSFM atlas to which the brain sample was aligned. (**e**) Example of the registration performed for one of the larger structures in the alignment between the brain sample and LSFM atlas. Images are taken from the yellow structure shown in the lower part of (**b**)-(**d**).

S2. **Accuracy of image registration**

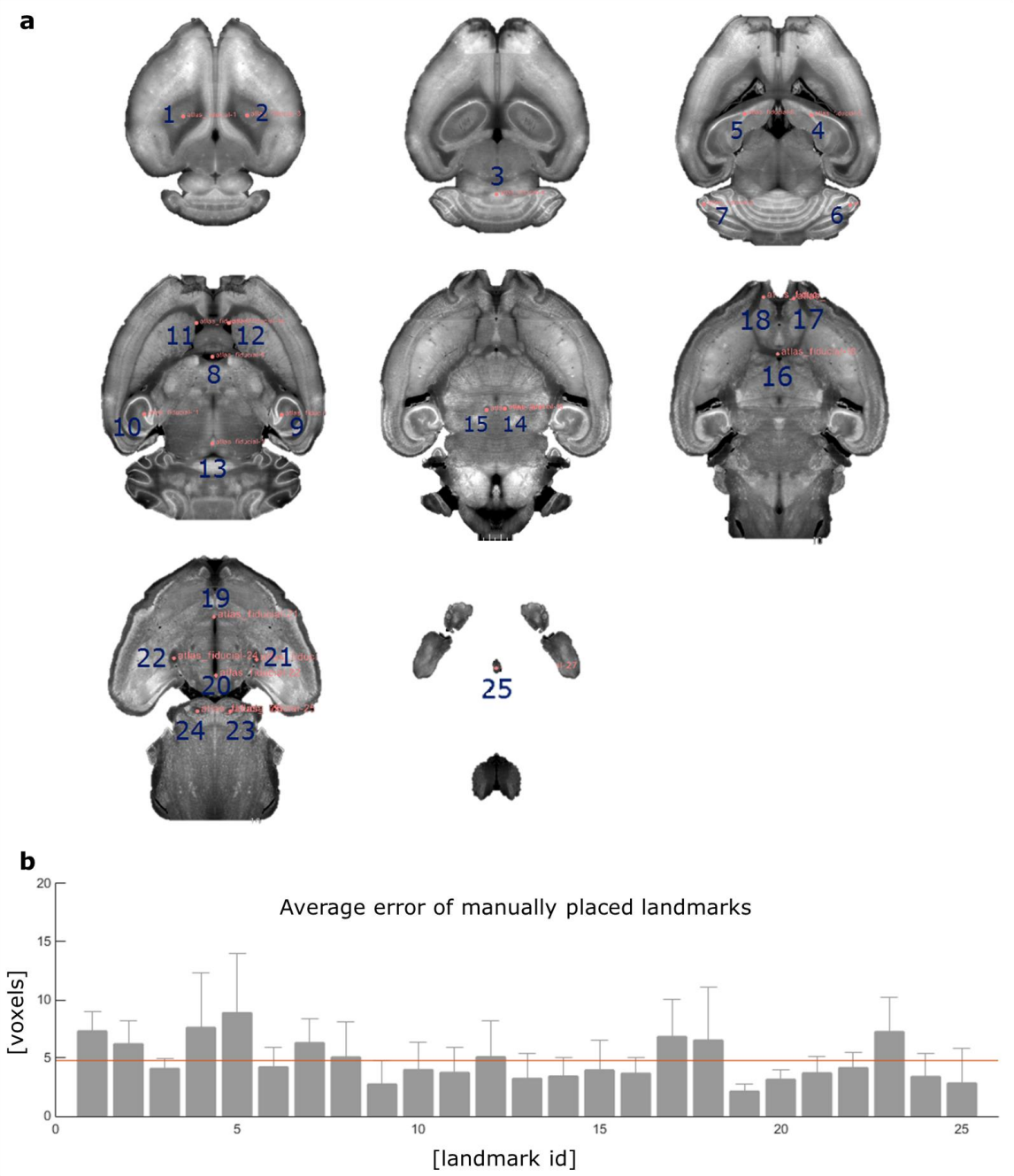

Supplement Figure2 I Accuracy of image registration. (**a**) The accuracy of the image registration for LSFM data was evaluated by manually placing 25 landmarks distributed throughout the LSFM template and comparing to corresponding landmarks placed in five brain samples after they had been registered to the LSFM template. Bar graph showing the mean error and standard deviation (n=5). The average error between the corresponding landmarks in samples and LSFM template was approximately 5 voxels corresponding to 100 µm.

S3. **Unmix signals**

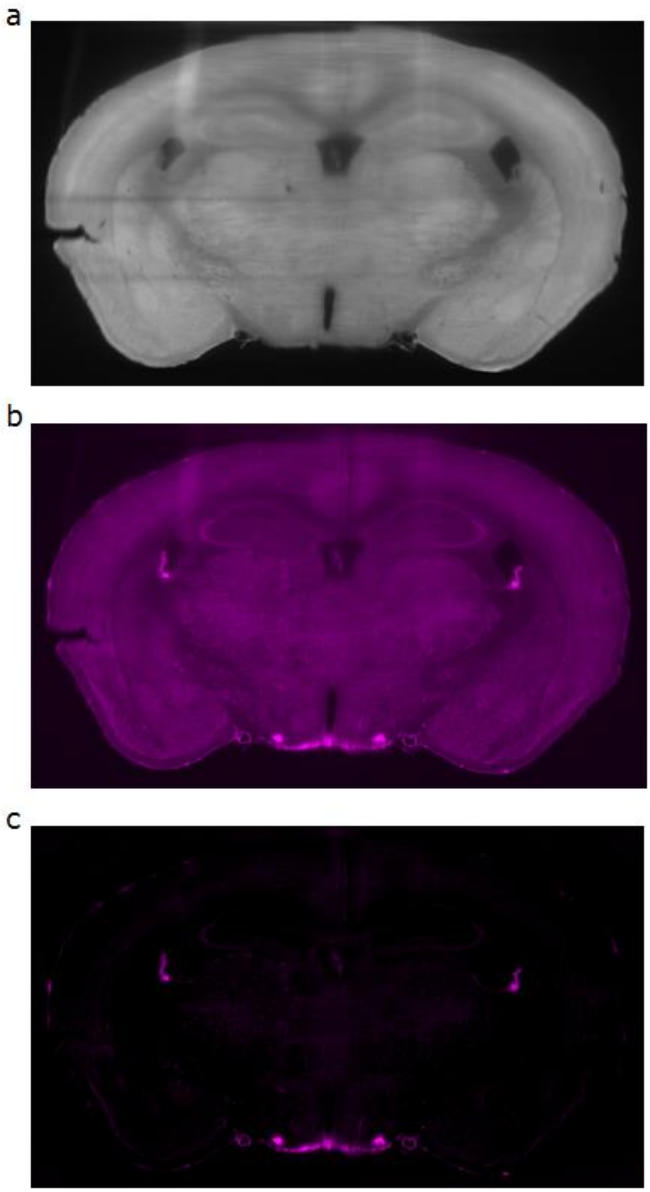

Supplement Figure 3 I Unmix signals. (**a**) Coronal projection of auto-fluorescence channel from liraglutide^{VT750} dosed animal acquired with LSFM. (**b**) Coronal projection of specific channel from liraglutide^{VT750} dosed animal. (**c**) Coronal projection of computed unmix channel from liraglutide^{VT750} dosed animal.

S4. **Average brain signals**

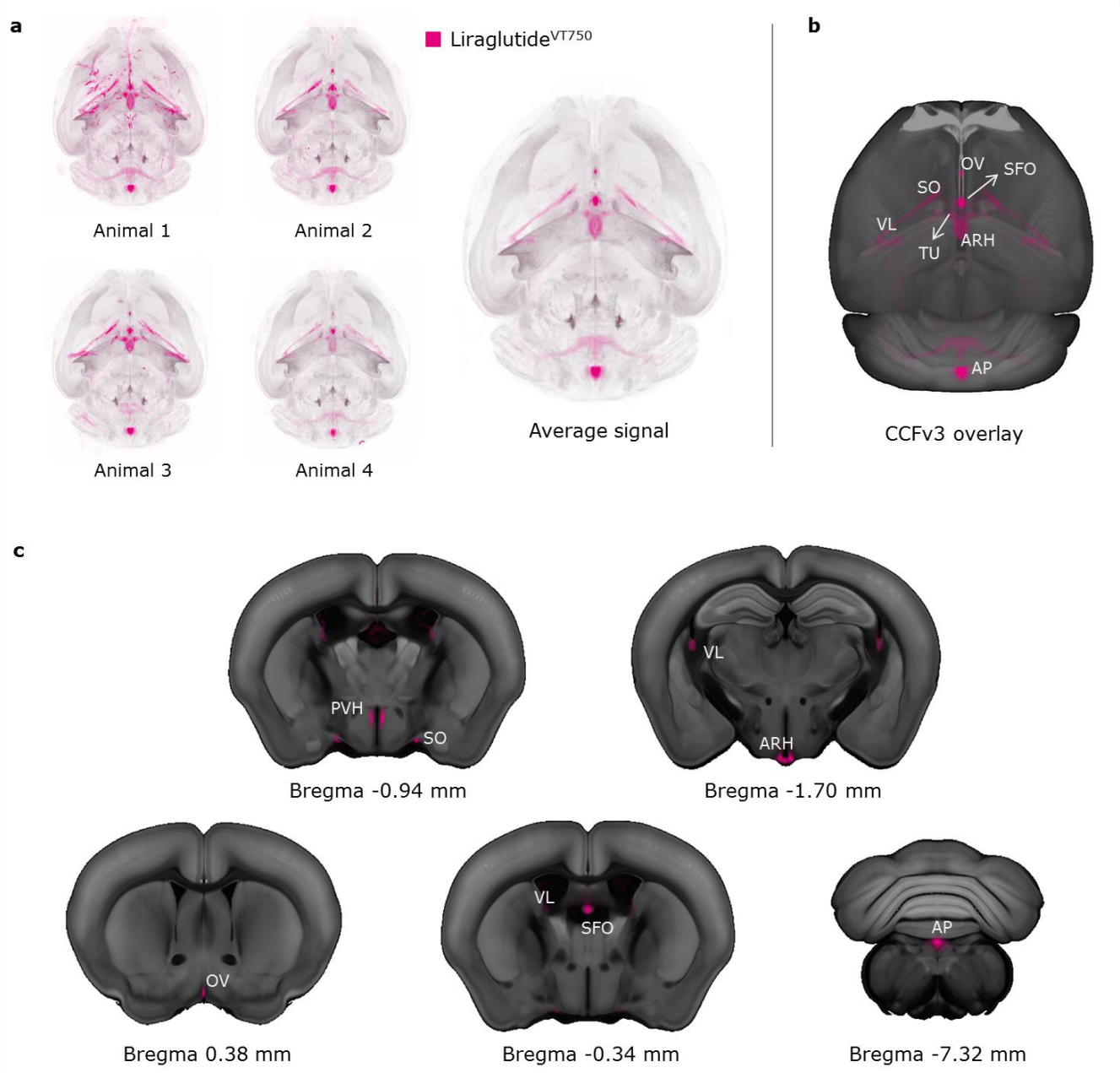

Supplement Figure 4 I Average brain signals. (**a**) Maximum intensity projection images of four individual brains from mice injected I.V. with liraglutide^{VT750}. The brains were registered to the atlas space and a voxel-wise average distribution signal representing the experiment group was computed. (**b**) The average signal from (a) overlaid onto the CCFv3 template[7]. (**c**) Coronal projection images constructed from (b). The color map was adjusted by a factor 2.5 in the top row to ease visualization of the lower signals in the non-circumventricular regions compared to the higher signals in the circumventricular regions (bottom row).

S5. **Confocal images of liraglutide^{Cy3}**

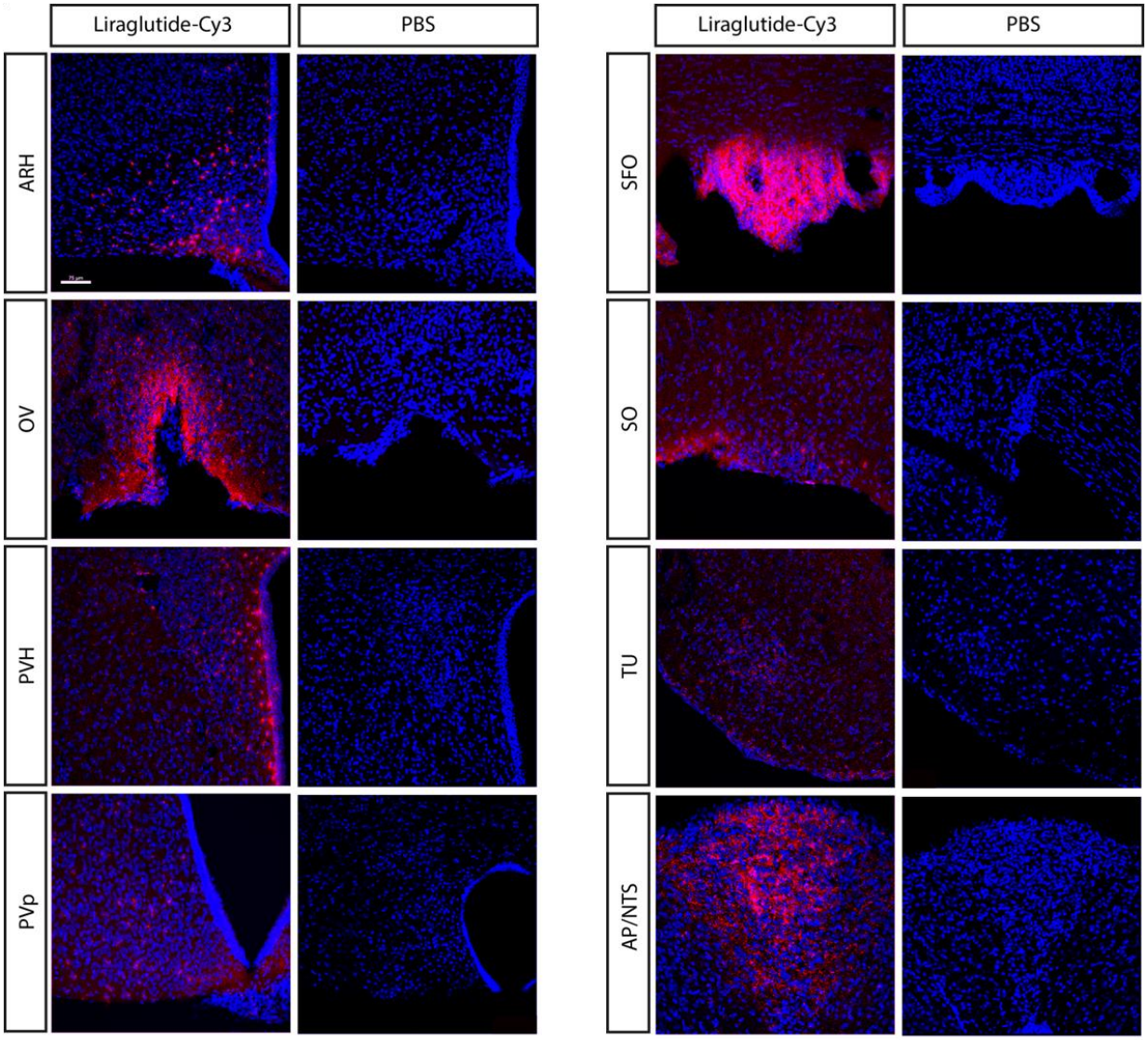

Supplement Figure 5 I Confocal images of liraglutide^{Cy3}. Overview of liraglutide^{Cy3} in the mouse brain. High magnification confocal images from mice injected with liraglutide^{Cy3}. Brain regions where liraglutide^{Cy3} (red) stained with DAPI nuclear stain (blue) were observed, compared to the corresponding region from an animal injected with vehicle (PBS).

S6. **Enhanced ISH images**

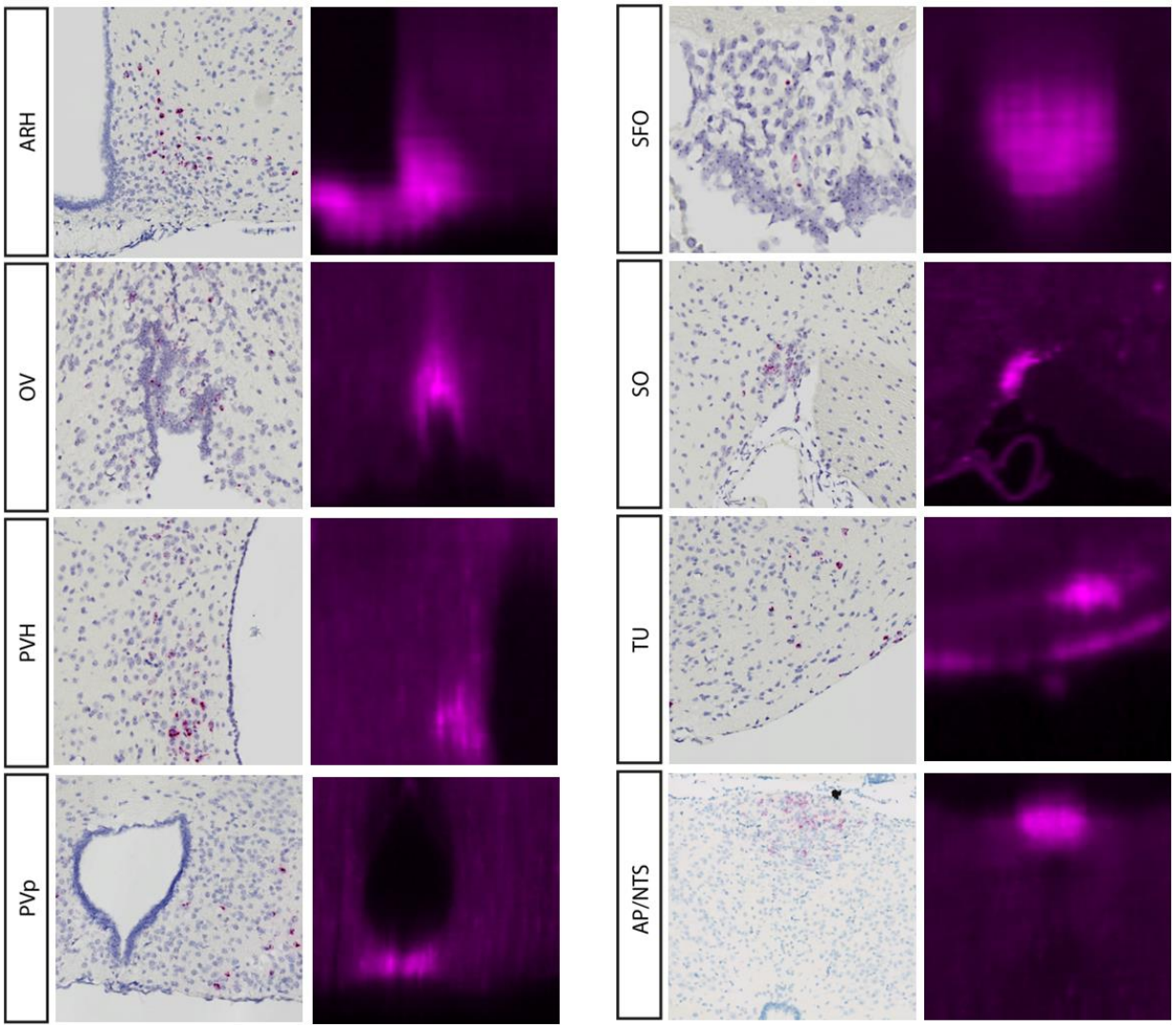

Supplement Figure 6 I Enhanced ISH images. Images show glp-1r expression in targeted brain regions. Overview of the glp-1r mRNA localization in a number of coronal sections throughout the C57/BL6 mouse brain. High magnification slide scanner images from untreated mice. Panel shows selected brain regions with glp-1r mRNA (red) counter stained with Mayer's hematoxylin (blue). The ISH images are compared to corresponding coronal projection images from a liraglutide^{VT750} distribution signal acquired with LSFM (pink).

S7. **Liraglutide^{VT750} in wild type vs *Glp-1r*$^{-/-}$ mice**

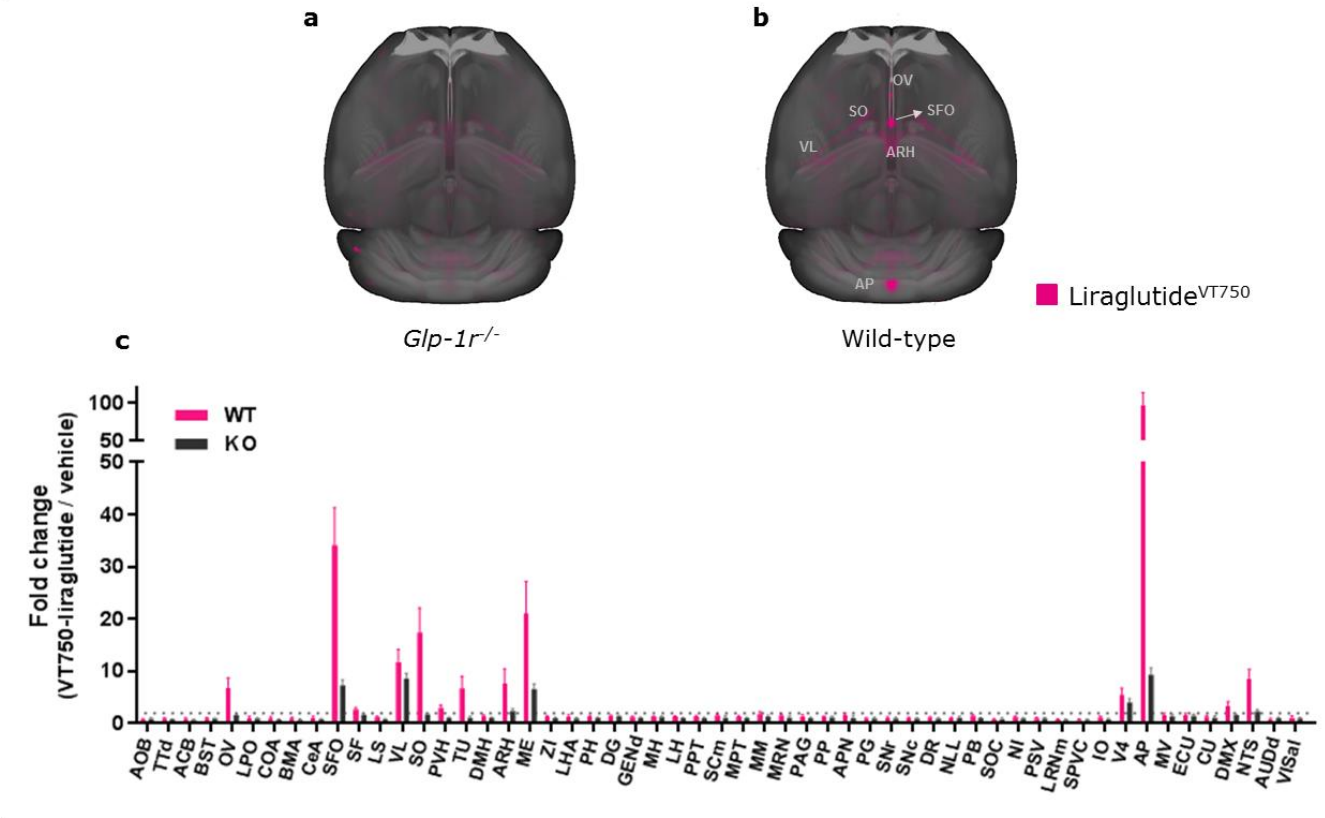

Supplement Figure 7 I Liraglutide^{VT750} in wild type vs *Glp-1r*$^{-/-}$ mice. (**a**) Maximum intensity projection of average liraglutide^{VT750} signal following administration in *Glp-1r*$^{-/-}$ animals overlaid onto the CCfv3 template[7]. (**b**) Maximum intensity projection of liraglutide^{VT750} signal following administration in wild-type animals overlaid onto the CCfv3 template[7]. (**c**) Bar graph showing mean fold change and standard deviation of vehicle normalized signals (total fluorescence) from liraglutide^{VT750} injected wild-type (WT) and *Glp-1r*$^{-/-}$ (KO) animals.

S8. **c-Fos heat maps**

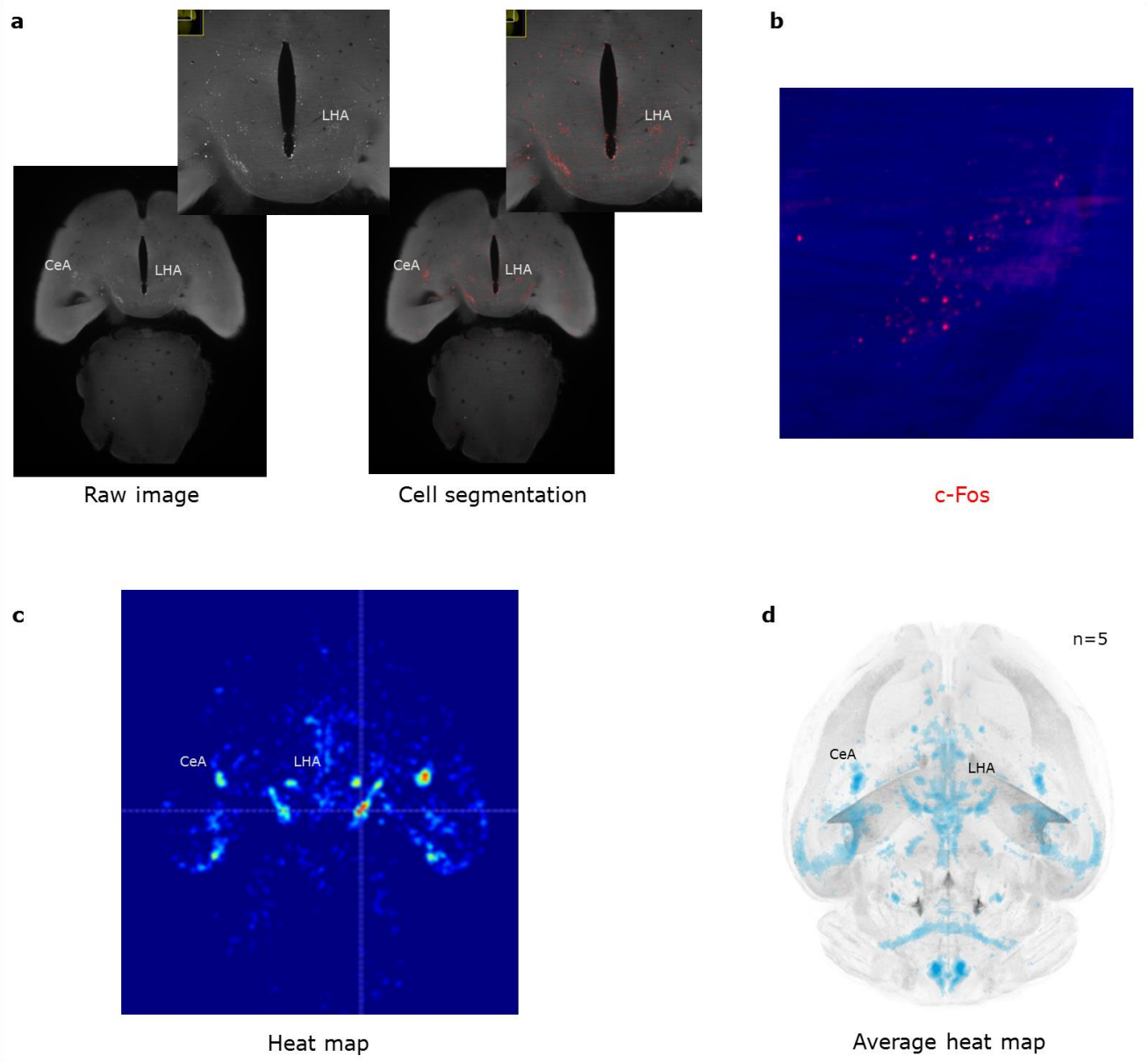

Supplement Figure 8 l c-Fos heat maps. (**a**) Raw LSFM image from a liraglutide injected mouse. The whole brain was stained for c-Fos prior to LSFM imaging. The red overlay shows the result of classifying cells positive for c-Fos. (**b**) High resolution image showing c-Fos positive cells (red). (**c**) c-Fos heat map constructed from the image seen in (a). Red color indicates high density of c-Fos positive cells. (**d**) Maximum intensity projection image of average c-Fos signal from five animals injected with liraglutide.

S9. **Rank plot**

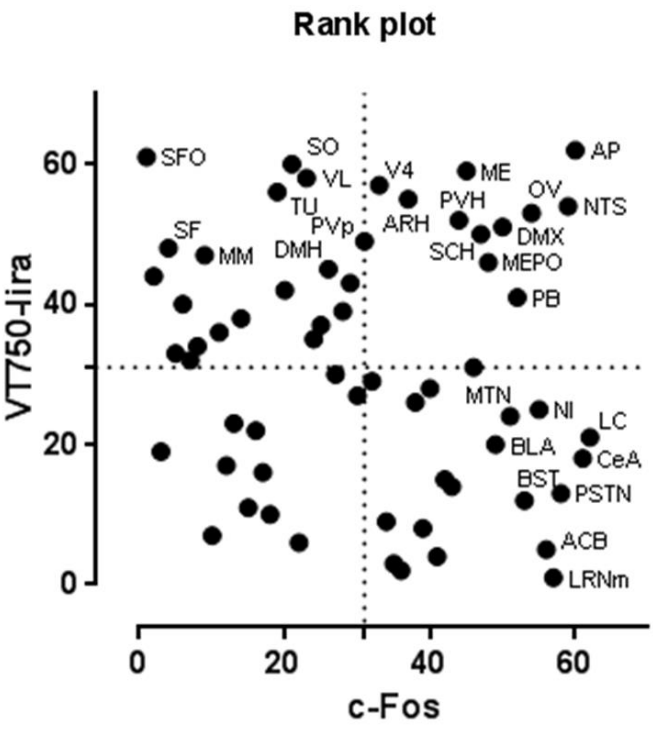

Supplement Figure 9 I Rank plot. Rank plot comparing c-Fos activation data from Fig. 4c with liraglutide^{VT750} distribution data from Fig. 2b. The brain regions were ranked based on their fold change value and these rankings were used as x and y coordinates in the plot. Top right corner contains brain regions where a direct activation from liraglutide is most plausible.

Supplementary Tables

Integrated Brain Atlas for Unbiased Mapping of Nervous System Effects Following Liraglutide Treatment

- T1. **Brain region abbreviations**
- T2. **Most overlapping connectivity maps from AIBS**
- T3. **Multiple t-tests, brain distribution**
- T4. **Multiple t-tests, brain activation**

T1. **Brain region abbreviations**

Abbreviation	Full name	Abbreviation	Full name
ACB	Nucleus accumbens	MM	Medial mammillary nucleus
AHN	Anterior hypothalamic nucleus	MPT	Medial pretectal area
AOB	Accessory olfactory bulb	MRN	Midbrain reticular nucleus
AP	Area postrema	MTN	Midline group of the dorsal thalamus
ARH	Arcuate hypothalamic nucleus	NI	Nucleus incertus
AUDd	Dorsal auditory area	NLL	Nucleus of the lateral lemniscus
BLA	Basolateral amygdalar nucleus	NTS	Nucleus of the solitary tract
BMA	Basomedial amygdalar nucleus	OV	Vascular organ of the lamina terminalis
BST	Bed nuclei of the stria terminalis	PAG	Periaqueductal gray
CA1	Field CA1	PB	Parabrachial nucleus
CA2	Field CA2	PCG	Pontine central gray
CA3	Field CA3	PG	Pontine gray
CEA	Central amygdalar nucleus	PH	Posterior hypothalamic nucleus
COA	Cortical amygdalar area	PSTN	Parasubthalamic nucleus
CU	Cuneate nucleus	PVH	Paraventricular hypothalamic nucleus
DG	Dentate gyrus	PVp	Periventricular hypothalamic nucleus, posterior part
DMH	Dorsomedial nucleus of the hypothalamus	PVT	Paraventricular nucleus of the thalamus
DMX	Dorsal motor nucleus of the vagus nerve	RE	Nucleus of reunions
DR	Dorsal nucleus raphe	RHP	Retrohippocampal region
ECT	Ectorhinal area	SCH	Suprachiasmatic nucleus
ECU	External cuneate nucleus	SCm	Superior colliculus, motor related
GENd	Geniculate group, dorsal thalamus	SF	Septofimbrial nucleus
GR	Gracile nucleus	SFO	Subfornical organ
IC	Inferior colliculus	SNc	Substantia nigra, compact part
LC	Locus ceruleus	SNr	Substantia nigra, reticular part
LH	Lateral habenula	SO	Supraoptic nucleus
LHA	Lateral hypothalamic area	TTd	Taenia tecta, dorsal part
LPO	Lateral preoptic area	TU	Tuberal nucleus
LRNm	Lateral reticular nucleus, magnocellular part	V4	fourth ventricle
LS	Lateral septal nucleus	VL	lateral ventricle
ME	Median eminence	VMH	Ventromedial hypothalamic nucleus
MEA	Medial amygdalar nucleus	VTA	Ventral tegmental area
MEPO	Median preoptic nucleus	ZI	Zona incerta
MH	Medial habenula		

Supplementary Table 1 I Brain region abbreviations. Full name of brain region abbreviations used in this manuscript. Brain region names follow the nomenclature of the AIBS CCFv3 atlas[7].

T2. **Most overlapping connectivity maps from AIBS**

Rank	Structure	Mouse line	Experiment id
1	NTS/DMX	Rasgrf2-T2A-dCre	310853453
2	CEA	C57BL/6J	112459547
3	PB	Calb2-IRES-Cre	183284388
4	PB	Slc17a6-IRES-Cre	305404551
5	GR/NTS	Gal-Cre_KI87	175816975
6	PB	Npr3-IRES2-Cre	545427588
7	PAG	Gad2-IRES-Cre	302053755
8	PB	Chat-IRES-Cre-neo	264565965
9	GR/NTS	C57BL/6J	159648854
10	AHN	Slc18a2-Cre_OZ14	301673462
11	PVT	Ntrk1-IRES-Cre	263106751
12	PB	Chat-IRES-Cre-neo	183901489
13	NTS/DMX	Pnmt-Cre	155735108
14	VMH/TU	C57BL/6J	112228391
15	CEA	Prkcd-GluCla-CFP-IRES-Cre	265945645
16	PVH	Tac1-IRES2-Cre	300888673
17	MEA	C57BL/6J	157550122
18	BST	Ppp1r17-Cre_NL146	267764292
19	NTS/DMX	Ppp1r17-Cre_NL146	268323342
20	NTS/DMX	Tac1-IRES2-Cre	180525136
21	DMH	Sim1-Cre	159222295
22	PVT	C57BL/6J	120875111
23	VMH/LHA	Erbb4-T2A-CreERT2	277854916
24	MEA	Adcyap1-2A-Cre	272819994
25	BLA/MEA	Crh-IRES-Cre_BL	277856332
26	AHN/LHA	Nos1-CreERT2	304998039
27	PVT	Grm2-Cre_MR90	183225830
28	CEA/MEA	Crh-IRES-Cre_ZJH	267152406
29	ARH	Pomc-Cre_BL	263369222
30	RE/PVH	Rasgrf2-T2A-dCre	310976160

Supplementary Table 2 I Most overlapping connectivity maps from AIBS. (**a**) List of the 30 most overlapping connectivity maps from AIBS compared to the liraglutide specific c-Fos increase following acute administration. The “Structure” column indicates the primary injection site where the virus used to trace the connections were injected. The “Mouse line” column indicates the mouse line used for the specific tracing experiment. The “Experiment id” column shows a unique AIBS id number for each experiment. All connectivity maps[6] were downloaded from the AIBS data portal.

T3. **Multiple t-tests, brain distribution**

Structure	Discovery?	P value	q value
AOB	No	0.298288	0.513718
AUDd	No	0.457365	0.659456
BLA	No	0.799363	0.875941
BMA	No	0.987891	0.987891
CA1	No	0.787127	0.875941
CA2	No	0.587313	0.74313
CA3	No	0.497779	0.679617
COA	No	0.778259	0.875941
DG	No	0.030414	0.099245
ECT	No	0.408925	0.618375
RHP	No	0.603671	0.748553
TTd	No	0.524749	0.690585
ACB	No	0.504232	0.679617
BST	No	0.855094	0.902401
CeA	No	0.701597	0.838174
LS	No	0.39843	0.617567
SF	Yes	0.004443	0.030606
ARH	Yes	0.009872	0.040806
DMH	Yes	0.0028	0.02893
LHA	No	0.080797	0.2178
LPO	No	0.494588	0.679617
ME	Yes	0.008816	0.040806
MEPO	No	0.099089	0.231437
MM	No	0.112884	0.236069
OV	Yes	0.005924	0.036731
PH	No	0.101531	0.231437
PSTN	No	0.858737	0.902401
PVH	Yes	0.001346	0.021867
PVp	Yes	0.007777	0.040184
SCH	No	0.265946	0.499657
SFO	Yes	0.00166	0.021867
SO	Yes	0.003336	0.029549
TU	Yes	0.009586	0.040806
VMH	No	0.114227	0.236069
ZI	No	0.097973	0.231437
GENd	No	0.015074	0.058412
LH	No	0.092259	0.231437
MH	No	0.019678	0.071766
MTN	No	0.160826	0.3116
DR	No	0.286786	0.508021

IC	No	0.274757	0.501027
MPT	No	0.129791	0.259582
MRN	No	0.10452	0.231437
PAG	No	0.064576	0.200184
SCm	No	0.079241	0.2178
SNc	No	0.874257	0.903398
SNr	No	0.716504	0.838174
VTA	No	0.317783	0.518488
LC	No	0.534646	0.690585
NI	No	0.31211	0.518488
NLL	No	0.805301	0.875941
PB	No	0.023846	0.082135
PCG	No	0.076102	0.2178
PG	No	0.964062	0.979866
AP	Yes	0.000099	0.006119
CU	No	0.33423	0.53134
DMX	Yes	0.00724	0.040184
ECU	No	0.708547	0.838174
LRNm	No	0.420513	0.620758
NTS	Yes	0.001763	0.021867
VL	Yes	0.000333	0.010334
V4	Yes	0.00411	0.030606

Supplementary Table 3 I Multiple t-tests, brain distribution. Statistical results of multiple t-tests on all brain regions from Figure 2b. Discovery was determined using the Original FDR method of Benjamini and Hochberg, with Q = 5%.Each row was analyzed individually, without assuming a consistent SD.

T4. **Multiple t-tests, brain activation**

Structure	Discovery?	P value	q value
AOB	No	0.649471	0.774369
AUDd	No	0.401123	0.604277
BLA	Yes	0.014399	0.117397
BMA	No	0.548283	0.686395
CA1	No	0.094397	0.36579
CA2	No	0.320452	0.584353
CA3	No	0.3919	0.604277
COA	No	0.849841	0.893053
DG	No	0.288082	0.541245
ECT	No	0.273741	0.53315
RHP	No	0.173924	0.448171
TTd	No	0.525741	0.686395
ACB	No	0.126403	0.385527
BST	Yes	0.013678	0.117397
CeA	Yes	0.0001	0.006214
LS	No	0.398816	0.604277
SF	No	0.200579	0.448171
ARH	Yes	0.028769	0.178601
DMH	No	0.372062	0.604277
LHA	No	0.235671	0.503848
LPO	No	0.13118	0.385527
ME	No	0.044773	0.252355
MEPO	No	0.1368	0.385527
MM	No	0.836736	0.893053
OV	No	0.094026	0.36579
PH	No	0.3795	0.604277
PSTN	Yes	0.003535	0.054791
PVH	No	0.124041	0.385527
PVp	No	0.102325	0.373186
SCH	No	0.083844	0.36579
SFO	No	0.275174	0.53315
SO	No	0.553544	0.686395
TU	No	0.474333	0.66812
VMH	No	0.393079	0.604277
ZI	No	0.519105	0.686395
GENd	No	0.976057	0.976057
LH	No	0.951222	0.966816
MH	No	0.81227	0.891098
MTN	Yes	0.015148	0.117397
DR	No	0.804906	0.891098

IC	No	0.484926	0.66812
MPT	No	0.819235	0.891098
MRN	No	0.536862	0.686395
PAG	No	0.873871	0.903
SCm	No	0.182647	0.448171
SNc	No	0.08842	0.36579
SNr	No	0.805588	0.891098
VTA	No	0.2024	0.448171
LC	Yes	0.001961	0.040529
NI	No	0.118438	0.385527
NLL	No	0.270209	0.53315
PB	Yes	0.028807	0.178601
PCG	No	0.158017	0.42596
PG	No	0.447606	0.645386
AP	Yes	0.008367	0.103745
CU	No	0.568752	0.691424
DMX	No	0.195675	0.448171
ECU	No	0.718	0.839924
LRNm	No	0.071984	0.36579
NTS	Yes	0.000793	0.024595
VL	No	0.409349	0.604277
V4	No	0.402187	0.604277

Supplementary Table 4 I Multiple t-tests, brain activation. Statistical results of multiple t-tests on all brain regions from Figure 5c. Discovery was determined using the Original FDR method of Benjamini and Hochberg, with Q = 20%.Each row was analyzed individually, without assuming a consistent SD.

Supplementary Movies

Integrated Brain Atlas for Unbiased Mapping of Nervous System Effects Following Liraglutide Treatment

- M1. **Comparing liraglutide^{VT750} brain distribution with liraglutide specific c-Fos increase**
- M2. **Comparing liraglutide specific c-Fos increase with AIBS connectivity maps**

M1. **Comparing liraglutide^{VT750} brain distribution with liraglutide specific c-Fos increase**

Average brain distribution of liraglutide^{VT750} (pink) overlaid with liraglutide specific c-Fos increase (blue). Signals were imported into the integrated brain atlas for visualization.

M2. **Comparing liraglutide specific c-Fos increase with AIBS connectivity maps**

Liraglutide specific c-Fos increase (blue) overlaid with glutamatergic projections from the parabrachial nucleus (yellow), and PKD-delta+ projections from the central amygdalar nucleus (red). Signals were imported into the integrated brain atlas for visualization.